# Collision of collisionless shocks – Part I: Hybrid PIC simulation & acceleration of the interplanetary shock in the magnetosheath

**C. Moissard[1], P. Savoini[1], D. Fontaine[1], R. Modolo[2]**

[1]Laboratoire de Physique des Plasmas (LPP), CNRS, Observatoire de Paris, Sorbonne Université, Université Paris Saclay, Ecole polytechnique, Institut Polytechnique de Paris, 91120 Palaiseau, France
[2]LATMOS, Sorbonne Université, 75005 Paris, France

**Key Points:**

- We perform the first self-consistent hybrid PIC simulation of the interaction between an interplanetary shock/sheath and the bow shock/magnetopause.
- We show that the interplanetary shock can accelerate in the magnetosheath – but only in the plane perpendicular to the interplanetary magnetic field.
- We note that the draping of the magnetic field lines along the magnetopause leads most interplanetary shocks to become locally quasi-parallel in the plane of the interplanetary magnetic field.

Corresponding author: Clément Moissard, `clement.moissard@york.ac.uk`

**Abstract**

A few MHD simulations have been performed to study the interaction between a propagating interplanetary shock and Earth's standing bow shock, followed by the magnetosheath and magnetopause. They satisfactorily explain the deceleration of the interplanetary shock in the magnetosheath, which was observed a few dozen times by well-arranged satellites. In this work, we perform a hybrid particle-in-cell simulation in a similar setting with a self-consistently developed quasi-perpendicular interplanetary shock. We track the position of the interplanetary shock as it travels through the magnetosheath. We show that early in the propagation through the magnetosheath, the interplanetary shock slows down, which is in line with the conclusion of previous studies. Later in the propagation, however, we find that – in the plane perpendicular to the interplanetary magnetic field – the interplanetary shock travels faster inside the magnetosheath than it does in the solar wind. We also note that as the magnetic field lines are stretched along the magnetopause, the interplanetary shock becomes quasi-parallel close to the magnetopause.

## 1 Introduction

The interaction between an interplanetary shock and the magnetosheath (delimited on either side by the bow shock and magnetopause) is difficult to observe *in-situ* because it ideally asks for at least five satellites at the right positions: four in the solar wind upstream of the bow shock to evaluate the orientation and velocity of the interplanetary shock, and one in the magnetosheath to observe its impact on the magnetosheath (*e.g.* Koval et al. (2005)). This is why only a few such observational studies exist on the subject (*e.g.* Koval et al. (2005); Koval, Šafránková, Němeček, Samsonov, et al. (2006); Koval, Šafránková, Němeček, and Přech (2006)). Even with such an ideally placed fleet of satellites, much extrapolation needs to be done to build a complete picture of the interaction. Numerical simulations allow us to build this global picture seamlessly, refer back to existing observations with a new perspective, and motivate new ones.

To our knowledge, an interplanetary shock followed by a sheath has never been introduced in a global numerical simulation. Interplanetary shocks themselves have been introduced, but not in a self-consistent manner, the usual approach being to introduce jump conditions, either following observational data or the Rankine-Hugoniot equations (*e.g.* Spreiter and Stahara (1992, 1994); Koval et al. (2005); Koval, Šafránková, Němeček, Samsonov, et al. (2006); Samsonov et al. (2006, 2007); Šafránková et al. (2007); Pallocchia et al. (2010)). These jump conditions artificially constrain the state of the plasma flow downstream of the interplanetary shock.

Previous numerical simulations and observations have shown that, in most cases, interplanetary shocks decelerate as soon as they enter the magnetosheath (*e.g.* Villante et al. (2004); Koval et al. (2005); Koval, Šafránková, Němeček, Samsonov, et al. (2006); Samsonov et al. (2006)). Koval et al. (2005); Koval, Šafránková, Němeček, Samsonov, et al. (2006) have attributed this deceleration to a smaller plasma bulk flow in the magnetosheath. We know, however, that under certain conditions, the plasma bulk flow can be faster on the flanks of the magnetosheath than in the solar wind (Chen et al., 1993; Lavraud et al., 2007, 2013). We used global numerical simulations to investigate the propagation of an interplanetary shock throughout the magnetosheath – paying special attention to the regions where the plasma bulk flow is accelerated.

We used the kinetic code (3D hybrid particle-in-cell) LatHyS (Modolo, 2004) and relaxed the hypotheses implied by the use of jump conditions when introducing an interplanetary shock in the simulation. The reason for using a kinetic code is to

check whether or not non-obvious kinetic effects appear in situations where they are traditionally not expected.

We introduced a magnetic cloud in the simulation box, following Burlaga (1988)'s model with the additional condition that the difference of speed between the magnetic cloud and the solar wind has to be faster than the upstream magnetosonic speed. This leads to the self-consistent formation of an interplanetary shock and sheath in the simulation. Then, we let this structure propagate through the simulation box and interact with a simulated geomagnetic environment that includes the bow shock, magnetosheath and magnetopause (see Turc et al. (2015) for a simplified example without the interplanetary shock).

In understanding this interaction, it is useful to divide the problem into two sub-problems. The first sub-problem is the evolution of the interplanetary shock as it is modified during its propagation through magnetosheath. The second one is the analysis of the impact of the interplanetary shock on the magnetosheath. In this article (Part I), we present our method for introducing a self-consistent interplanetary shock together with a self-consistently developed geomagnetic environment (bow shock, magnetosheath, magnetopause) in Hybrid particle-in-cell simulations. Then, we focus on the first sub-problem of tracking the interplanetary shock throughout the magnetosheath. A following article (Part II) will address the second sub-problem of the evolution of the magnetosheath following its encounter with the interplanetary shock and sheath. The remainder of this paper is organised as follows:

In section 2, we briefly present the global setup used in the hybrid PIC code LatHyS (Modolo, 2004; Turc et al., 2015) to self-consistently model the geomagnetic environment (bow shock, magnetosheath, magnetopause). Then we describe our method for introducing a magnetic cloud in the simulation box and how its interaction with the solar wind leads to the self-consistent formation of a satisfactorily realistic interplanetary shock followed by a sheath. The results reported in section 3 are split into two parts. In the first part, we focus on the propagation of the interplanetary shock through the magnetosheath. In the second part, we briefly comment on the configuration of the magnetic field in the magnetosheath. Finally, sections 4 and 5 are dedicated to the interpretation of these results.

## 2 Method

Figure 1 is a concept diagram of our simulation setup. On the right-hand side of the box, we place an obstacle consisting of a magnetic dipole and an absorbing sphere, while on the left-hand side of the box, we inject a magnetic cloud using an analytical expression. The obstacle's interaction with the solar wind self-consistently generates a bow shock, a magnetopause, with a magnetosheath in between these two frontiers (see subsection 2.1 of the present article and Turc et al. (2015)). The magnetic cloud propagates through the solar wind, overtaking the bulk plasma to self-consistently generate a shock and sheath (see subsection 2.2).

### 2.1 The geomagnetic environment

We used the 3D hybrid PIC code Lathys (Modolo, 2004), and used a setup similar to, albeit significantly larger than Turc et al. (2015). The box dimensions are 1500 cells in the X direction, 720 cells in the Y direction and 660 cells in the Z direction. Each grid cell is a cube of dimension $(1\ d_i)^3$, where $d_i \sim 92$ km is the ion skin depth computed from the initial solar wind values. Therefore, we will talk interchangeably about $x$, $y$ and $z$ in terms of cell numbers or in terms of $d_i$.

The "planet" (Earth) is represented in the code by a magnetic dipole placed at the origin ($x = 0$, $y = 0$, $z = 0$). The magnetic moment was chosen as $M =$

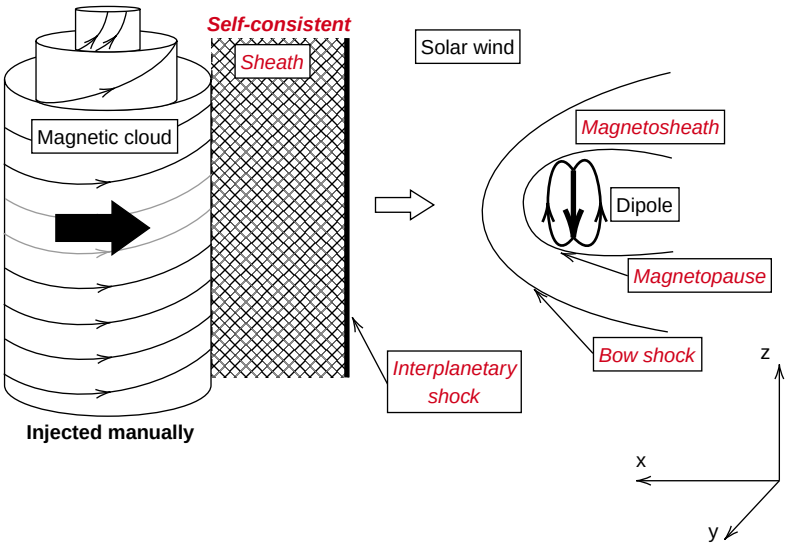


**Figure 1.** Simulation setup. A magnetic cloud is injected into the simulation box. It interacts with the solar wind to self-consistently create a shock and sheath. These structures interact with the geomagnetic environment, which itself results self-consistently from the interaction between the solar wind and a magnetic dipole. Structures that are injected (described by analytical expressions in the code) are noted in black. Structures that develop self-consistently are noted in red.

$900 \cdot 10^9 (\mathrm{nT}) \times (14\ d_i)^3$. This allows the magnetopause position, accordingly to the simple dynamic pressure/magnetic pressure balance (Schield, 1969), to be 34 $d_i$. This is safely above the 20 $d_i$ threshold, which Omidi et al. (2004) showed to be a lower limit above which a simulated obstacle – or a real celestial body – interacting with the solar wind would display a similar magnetosphere to Earth's.

This magnetic dipole interacts with a simple model for the solar wind: from the left side of the simulation box ($x > 0$), we inject a supersonic/superalfvénic plasma of protons neutralised by a massless electron fluid of density $N = 6$ (ions/cm$^{-3}$) with a bulk speed of $V_{\mathrm{SW}} = 400$ km/s, carrying a magnetic field $B = 10$ nT. The ions have a Maxwellian distribution of velocities corresponding to a temperature chosen to have $\beta = 0.5$ for plasma beta of the solar wind. These values are typical of the observed solar wind (e.g. Venzmer and Bothmer (2018)). The interplanetary magnetic field is parallel to the ecliptic ($xy$) plane and makes an 85° angle with the $x$ direction, with $B_x > 0$ and $B_y > 0$.

After 190 $\left(\Omega_{\mathrm{ci}}^{-1}\right)$[1], the interaction between the solar wind and the magnetic dipole leads to the self-consistent formation of a magnetosheath, delimited on each side by a bow shock and a magnetopause. We recover the main characteristics of Earth's magnetosheath: the plasma is subalfvénic in the nose of the magnetosheath, then it is diverted and recovers a superalfvénic velocity on the flanks (Lucek et al., 2005); the plasma beta is of the order of unity, and the total pressure close to 1 nPa (Lin et

[1] Throughout this text, $\Omega_{\mathrm{ci}}^{-1} \sim 1$ s serves as the time unit and refers to the inverse of the cyclotron pulsation computed from the initial magnetic field amplitude in the solar wind: $B = 10$ nT.

al., 1991), the shape of the bow shock and magnetopause are realistic (see Turc et al. (2015) for details).

In particular, we find that the plasma can be faster in the magnetosheath (close to the magnetopause in the plane perpendicular to the interplanetary magnetic field) than it is in the solar wind. This effect is well documented (see *e.g.* Chen et al. (1993); Lavraud et al. (2007, 2013)). On figure 2, we can see that indeed, $v_{bulk} \sim 450$ km/s close to the magnetopause, while $v_{bulk} \sim 40$ km/s in the solar wind.

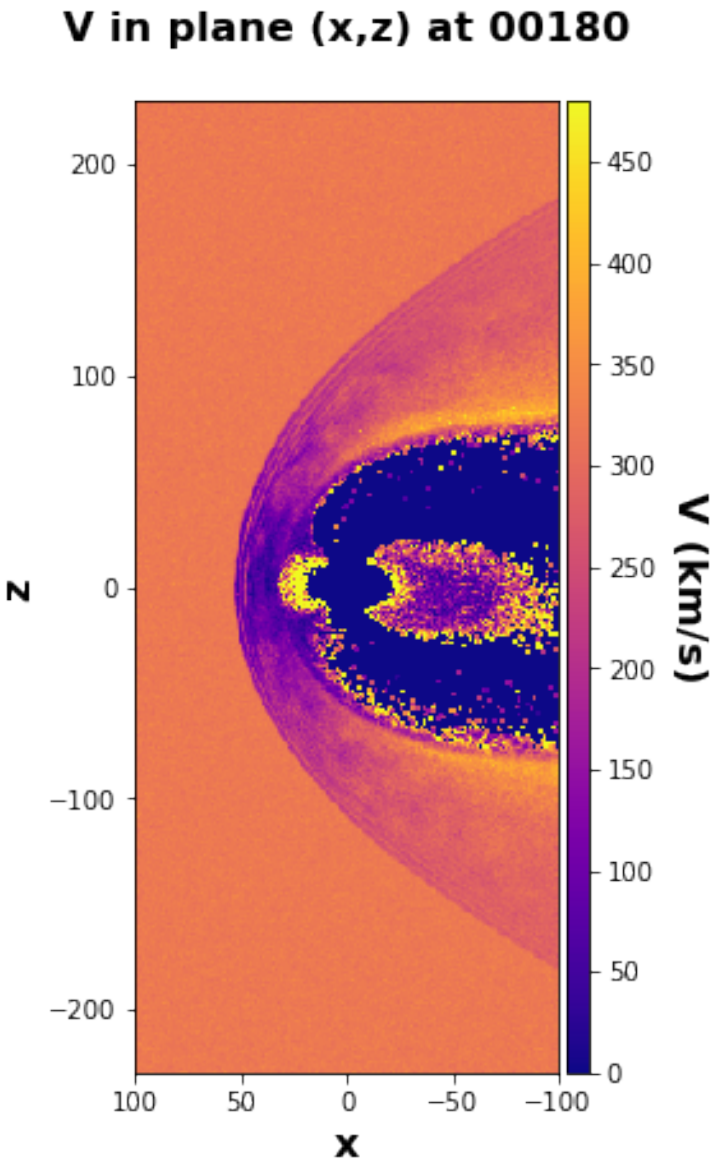


**Figure 2.** Colormap of the bulk velocity in the noon-midnight meridian plane, which is also the plane perpendicular to the interplanetary magnetic field. This figure represents the state of the geomagnetic environment prior to its encounter with the interplanetary shock and sheath

.

### 2.2 The magnetic cloud-driven sheath

#### *2.2.1 The magnetic cloud*

To create a shock and its sheath in front of the injected magnetic cloud, we introduced this structure at the entry plane and let it propagate in the simulation box. We chose the velocity $V_{\mathrm{MC}}$ of the introduced magnetic cloud to be fast enough that its propagation led to the formation of a shock wave: $V_{\mathrm{MC}} - V_{\mathrm{SW}} > V_{\mathrm{A}}$, where $V_{\mathrm{A}}$ is the Alfvén speed.

Magnetic clouds are truly gigantic structures compared to Earth's geomagnetic environment: a typical magnetic cloud has a size of 1/3 AU (Lepping et al., 2006) by the time it reaches Earth. This allows us to consider the magnetic cloud as a planar structure in our simulations. For simplicity, we make the hypothesis that the magnetic cloud lies in the (yz) plan, *i.e.* its collision with Earth is frontal. This would be the case for a magnetic cloud heading directly toward Earth from the Sun.

The widely used model of Burlaga (1988) describes a magnetic cloud as a force-free structure, with the magnetic field components proportional to the first two Bessel functions ($J_0$ and $J_1$):

$$\begin{aligned} B_A &= B_0 J_0(ar) \text{ (Axial component)} \\ B_T &= B_0 H J_1(ar) \text{ (Tangential component)} \\ B_R &= 0 \text{ (Radial component)} \end{aligned} \tag{1}$$

$B_0$ is the amplitude of the magnetic field at the centre of the magnetic cloud, $r$ is the distance from the magnetic axis of the flux rope, $a$ determines the size of the magnetic cloud, and $H$ can be chosen as $\pm 1$ depending on the handedness of the flux rope. We chose $H = 1$.

These equations describe the magnetic field in space. In contrast, in our simulation, we introduced the magnetic cloud over time from the left edge of the box and let it propagate into the simulation volume. The point is to let everything inside of the simulation box evolve self-consistently. We, therefore, rewrote equations 1 in terms of time rather than radius:

$$\begin{aligned} B_z(t \leq t_0) = B_A(t \leq t_0) &= B_0 J_0(a \cdot u_0(t - t_0) - 2.4) \text{ (Axial component)} \\ B_y(t \leq t_0) = B_T(t \leq t_0) &= B_0 J_1(a \cdot u_0(t - t_0) - 2.4) \text{ (Tangential component)} \\ B_x(t \leq t_0) = B_R(t \leq t_0) &= Constant \text{ (Radial component)} \end{aligned} \tag{2}$$

In these equations, $u_0$ is the bulk flow velocity, $t_0$ is the time at which we start injecting the magnetic cloud, and $t$ is the time in the simulation. The 2.4 offset is used to make $t_0$ the start of the magnetic cloud since $J_0(2.4) = 0$.

In our simulation, we chose the axial component of the cloud to be along the $z$ axis and the tangential component to be along the $y$ axis (see figure 1). We consider the case of a planar magnetic cloud travelling along the $x$ direction and crossed at its centre; therefore the $x$ axis crosses the magnetic cloud radially. For simplicity, we decided to make the magnetic field (as well as the velocity, temperature, and density) homogeneous on the whole entry plane, *i.e.* $\frac{\partial}{\partial y} = \frac{\partial}{\partial z} = 0$. Since $B_x$ is constant at the entry plane, it follows straightforwardly that the introduced magnetic field verifies flux conservation. The other Maxwell equations are built into the hybrid scheme.

We decided to use a northward axial magnetic field. The most interesting impacts of our event on the geomagnetic environment should therefore come from the interplanetary shock and sheath rather than from the magnetic cloud. Indeed, choosing the axial component to be northward excludes the already well studied magnetic reconnection effects that occur when a southward magnetic field interacts with the magnetopause (Dungey, 1961; Fairfield & Cahill, 1966; Tsurutani et al., 2020).

Using only equations (2) to describe the evolution of the magnetic field would lead $B_T$ to start too abruptly, from whichever value it had in the solar wind, to $B_T = B_0 H J_1(-2.4) \neq 0$. The same would be true for the $B_A$, which would abruptly go from its solar wind value to 0. These jumps would lead to numerical problems, so we introduced a smooth ramp, using $\tau_0$ to control the sharpness of the transition from quiet solar wind conditions to magnetic cloud conditions:

$$\begin{aligned} B_A(t < t_0) &= B_{zSW} + (0 - B_{zSW})\frac{1}{2}\left(1 + \tanh\left(\frac{t - t_0}{\tau_0}\right)\right) \\ B_T(t < t_0) &= B_{ySW} + (B_0 J_1(-2.4) - B_{ySW})\frac{1}{2}\left(1 + \tanh\left(\frac{t - t_0}{\tau_0}\right)\right) \end{aligned} \tag{3}$$

To our knowledge, there is no available analytical model for the velocity and temperature of the plasma in a magnetic cloud. We know, however, that the plasma in a magnetic cloud is generally much colder than in the solar wind, but has a similar density (Regnault et al., 2020). In order to create a shock and sheath, we also need the magnetic cloud to be faster than the solar wind by at least the Alfvén speed. Finally, we know that the magnetic cloud is a passing structure, so the plasma conditions should return to those of the solar wind after its passage. In order to take into account these observations, we introduce the plasma with a bulk speed $V(t)$ and a thermal speed $V^{\mathrm{th}}(t)$ as follows:

$$V(t) = V_{\mathrm{SW}} + (V_{\mathrm{MC}} - V_{\mathrm{SW}}) \times \left(\tanh\frac{t - t_0}{\tau_0} - \tanh\frac{t - t_1}{\tau_1}\right) \tag{4}$$

$$V^{\mathrm{th}}(t) = V^{\mathrm{th}}_{\mathrm{SW}} + (V^{\mathrm{th}}_{\mathrm{MC}} - V^{\mathrm{th}}_{\mathrm{SW}}) \times \left(\tanh\frac{t - t_0}{\tau_0} - \tanh\frac{t - t_1}{\tau_1}\right) \tag{5}$$

The subscript SW refers to the value of the subscripted quantity in the quiet solar wind, whereas MC refers to its value in the magnetic cloud. $t_0$ is when the piston starts, and $t_1$ the time at which it ends, while $\tau_0$ and $\tau_1$ control the sharpness of the transition from quiet solar wind conditions to magnetic cloud conditions and back. We used the same $t_0$ and $\tau_0$ as for the ramp of the magnetic field.

This is a particle-in-cell in code, therefore the quantities $V(t)$ and $V_{\mathrm{th}}(t)$ are used to compute the velocity distribution of the injected ions.

#### *2.2.2 Summary of the simulation setup*

Tables 1 and 2 summarise the simulation setup.

| | |
|---|---|
| dx, dy, dz | 1 $d_i$ |
| dt | 0.005 $\Omega_{\mathrm{ci}}^{-1}$ |
| tmax | 300 $\Omega_{\mathrm{ci}}^{-1}$ |
| Nx | 1500 |
| Ny | 720 |
| Nz | 660 |
| N procs | 7200 |
| N particles | $\sim 15 \cdot 10^9$ |
| computing time | $\sim$ 300.000 hours |

**Table 1. Simulation parameters**

Figure 3 summarises the temporal evolution of the plasma conditions at the injection side of the box. The horizontal axis represents time: the values plotted are

| | Solar wind | Magnetic cloud |
|---|---|---|
| B (nT) | 10 | 50 |
| B orientation | $B_x = B\cos(85°) \mid B_y = B\sin(85°) \mid B_z = 0$ | Axial field: $B_z$ \| Tangential field: $B_y$ |
| V (km/s) | 400 | 750 |
| N (ions/cm$^{-3}$) | 6 | 6 |
| T (K) | 240k | 24k |

**Table 2. Macroscopic parameters**

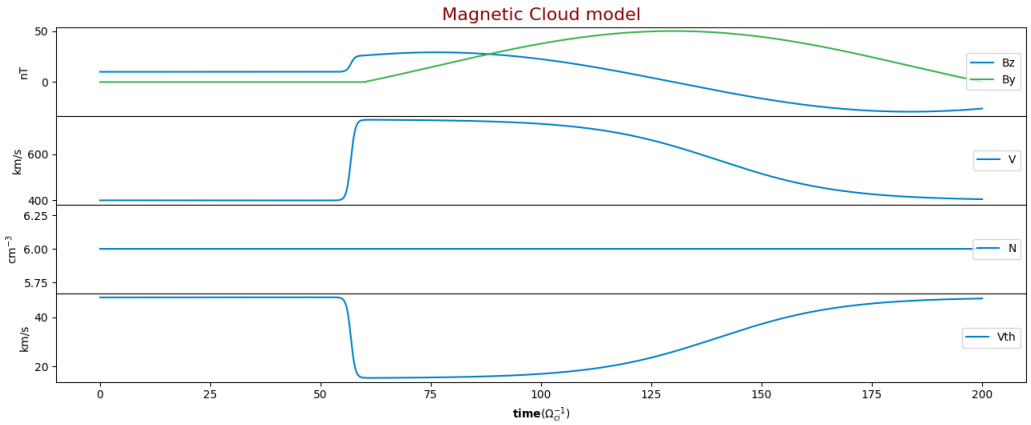


**Figure 3.** From top to bottom: the magnetic field's $y$ and $z$ components, bulk velocity, density and thermal velocity. These are the characteristics of the plasma injected at the left side of the simulation box and their temporal evolution.

what we inject in the simulation box, which will then develop according to the physics captured by LatHyS' numerical scheme.

The magnetic cloud is injected from $t = 70\ \Omega_{\rm ci}^{-1}$ so that the interplanetary shock formed by its interaction with the quiet solar wind reaches the bow shock around $t = 216\ \Omega_{\rm ci}^{-1}$, *i.e.* after the magnetosheath had the time to reach a stationary state (for $t \geq 190\ \Omega_{\rm ci}^{-1}$).

### *2.2.3 The interplanetary shock and the sheath*

Figure 4 shows the structure self-consistently produced by the propagation of the magnetic cloud as it overtakes the solar wind, at $t = 200\ \Omega_{\rm ci}^{-1}$. The figure is plotted along the spatial $x$-axis. For clarity, the geomagnetic environment has been excluded from the plot. From right to left, we can see: a stretch of solar wind, then the shock, followed by the sheath, and eventually the magnetic cloud.

The shock presents an Alfvén Mach number of $M_A = \frac{v_s - v^{up}}{v_A^{up}} = 4.2$; where $v_s$ is the velocity of the shock in the GSE frame, $v^{up}$ and $v_A^{up}$ are, respectively, the velocity of the bulk plasma and the Alfvén speed upstream of the shock. The sheath thus obtained numerically captures the main characteristics of observed sheaths (e.g. Kilpua et al. (2017)): the magnetic field amplitude, velocity, density and temperature are significantly higher than in the solar wind. The plasma beta is also elevated, which is a consequence of significant heating at the shock. We can also see that the

plasma quantities in the sheath fluctuate more than they do in the solar wind, which is expected (Moissard et al., 2019).

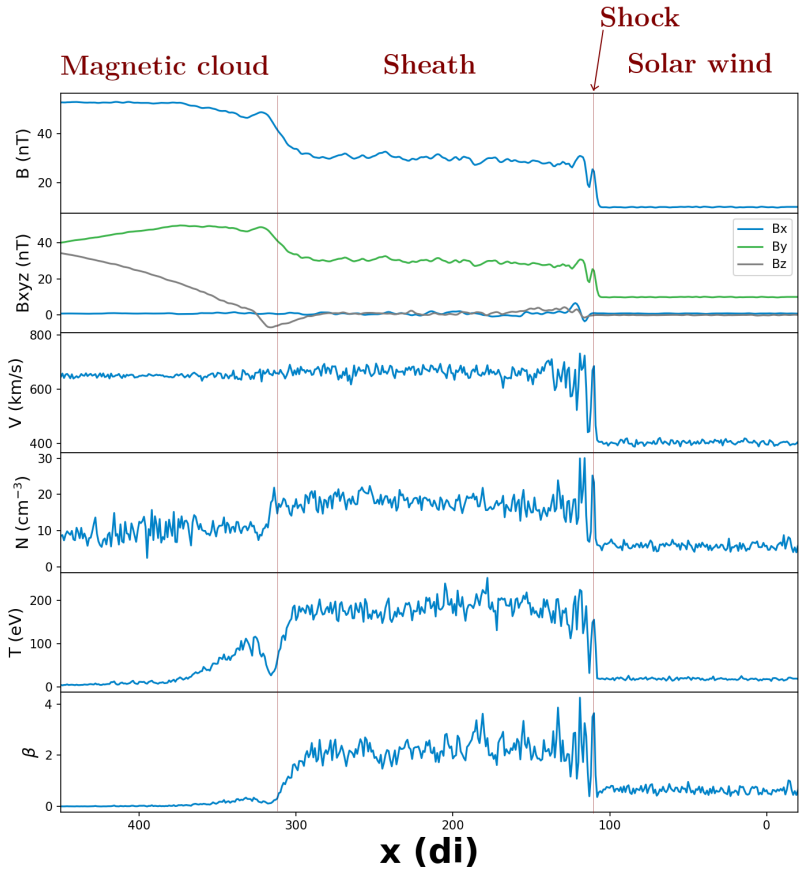


**Figure 4.** Main plasma parameters in the self-consistently created sheath at time = 210 $\Omega_{ci}^{-1}$, shortly before its encounter with Earth. For clarity, Earth's geomagnetic environment has been removed from this plot. Earth's centre would be located at $x = 0$.

# 3 Results

This section focuses on the interplanetary shock as it travels through the magnetosheath.

## 3.1 The curvature of the interplanetary shock

### *3.1.1 From the bow shock to the magnetopause*

The interplanetary shock slows down as soon as it penetrates the magnetosheath. This braking is not negligible, but not large either. Naturally, the parts of the interplanetary shock that cross the bow shock the earliest have more time to travel at a reduced speed than the parts which enter later. This leads to a slight curvature of the interplanetary shock. Figure 5 shows the density in the ecliptic plane ($(xy)$ plane, with $z = 0$) just before the collision between the interplanetary shock and the bow shock (left panel) and just before its collision with the magnetopause (right panel). On the right panel, we can see that the interplanetary shock has become slightly curved as it travelled through the magnetosheath.

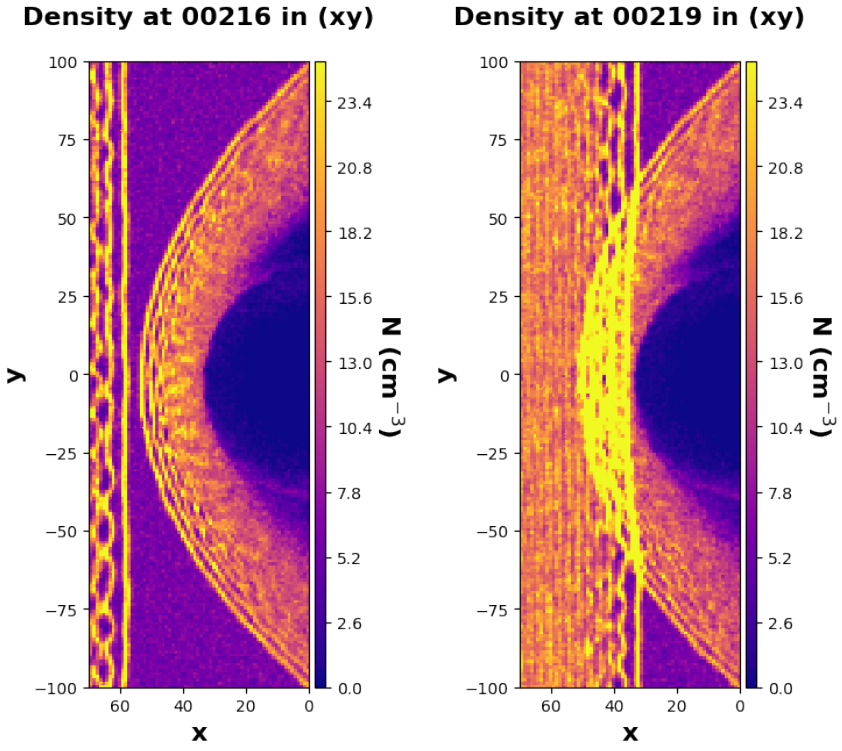


**Figure 5.** Density in the ecliptic plane. Left panel: soon before the shock/shock collision. Right panel: soon before the interplanetary shock/magnetopause collision.

In the simulation, it takes 3.5 $\Omega_{ci}^{-1}$ for the interplanetary shock to travel from the nose of the bow shock to the nose of the magnetopause. Translated into observational time ($\Omega_{ci}^{-1}$ corresponds to 1 second, the scale of the simulation is $1/16^{th}$ that of reality), it would take $3.5 \times 1 \times 16 = 56$ seconds for the interplanetary shock to travel from the bow shock to the magnetopause (versus 45 seconds if it kept travelling at the speed it had outside of the magnetosheath). This is a much shorter time than the estimations made by Villante et al. (2004) who found that it would take between 4 and 7 minutes

for radially propagating shocks to cross the magnetosheath. Their study, however, included only relatively slow shocks (20 shocks from 220 to 470 km/s, with most of them between 300 and 400 km/s), whereas our shock travels at 780 km/s.

Villante et al. (2004) estimated that the speed of the shock in the magnetosheath would fall between 1/4 and 1/3 to what it was in the solar wind – which would lead to a severe curvature of the interplanetary shock in the magnetosheath. Since then, a few observational (*e.g.* Koval et al. (2005); Koval, Šafránková, Němeček, Samsonov, et al. (2006); Koval, Šafránková, Němeček, and Přech (2006)) and numerical (Koval et al., 2005; Koval, Šafránková, Němeček, Samsonov, et al., 2006; Samsonov et al., 2006, 2007; Šafránková et al., 2007; Pallocchia et al., 2010) studies have found much softer deceleration (between 10 and 30% at most), which is more in line with the results reported here.

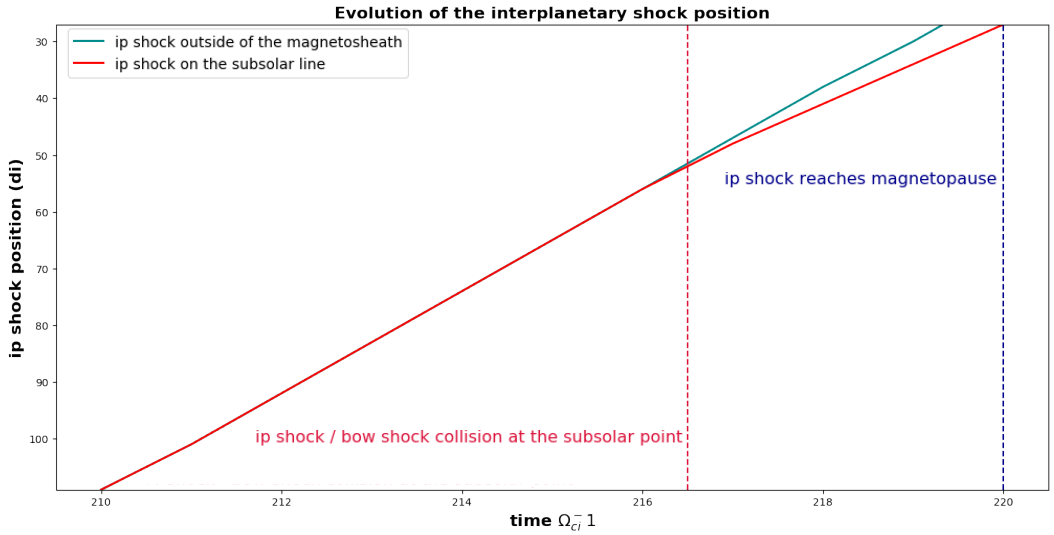


**Figure 6.** Blue line: position of the unperturbed interplanetary shock, as followed outside of the magnetosheath. Red line: position of the interplanetary shock as followed along the Sun-Earth line ($y = z = 0$) until it reaches the magnetopause at $t = 220\ \Omega_{\rm ci}^{-1}$. The two dashed vertical lines indicate the arrival of the interplanetary shock at the nose of the bow shock (red) and, later, at the nose of the magnetosheath (blue).

In figure 6, we plot the position of the interplanetary shock front against time. The red line represents the position of the shock front along the Sun-Earth line, where it interacts with the nose of the bow shock, magnetosheath and magnetopause. The blue line is the position of the shock in a part of the simulation where it does not interact with the geomagnetic environment and thus serves as a reference. The vertical dashed lines mark the time of collision between the interplanetary shock and the bow shock (red dashes) or its collision with the magnetopause (blue dashes).

The braking of the interplanetary shock from the moment it penetrates inside the magnetosheath (at $t = 216.5\ \Omega_{\rm ci}^{-1}$) is clear on this figure. We also see that, as noted by Pallocchia et al. (2010), most of the braking seems to happen at the moment the interplanetary shock enters the magnetosheath: its velocity does not change much after the initial change of speed. From this figure, we can compute that the speed of the interplanetary shock inside of the magnetosheath is 0.8 times its speed before the collision. This falls into the 0.73-0.97 range established by Koval, Šafránková, Němeček, and Přech (2006) through satellite observations.

### *3.1.2 On the flanks of the magnetopause*

We ran the simulation significantly further in time and let the interplanetary shock propagate through the flanks of the magnetosheath.

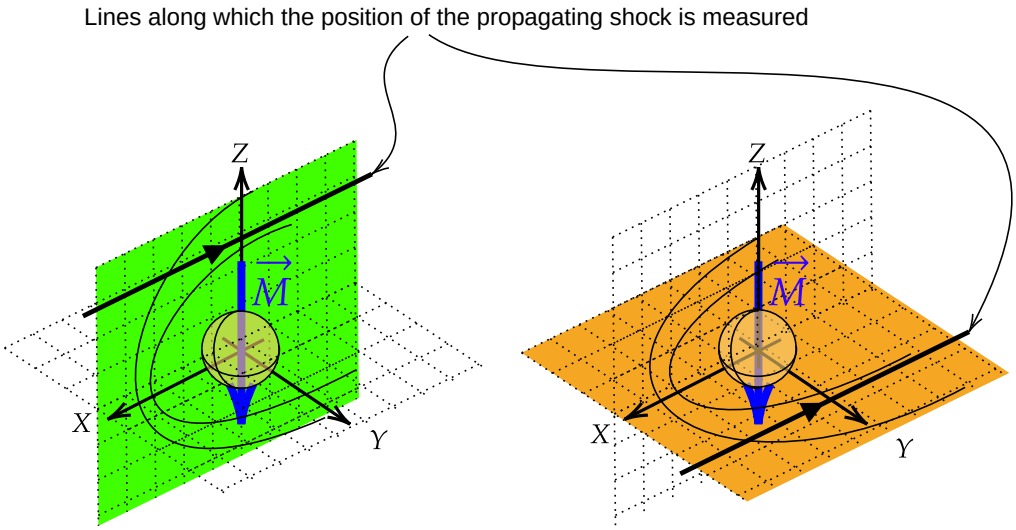


**Figure 7.** The beige sphere represents the obstacle modelling Earth. Left panel: the noon-meridian plane, in green. Right panel: the ecliptic plane, in orange. Thick black lines with an arrow show where we tracked the position of the propagating shock front.

Figure 7 is a sketch that shows two planes that cut through the simulation box: the noon-midnight meridian plane in green and the ecliptic plane in orange. In this subsection, we follow the position of the interplanetary shock as it travels through the magnetosheath on the flanks of the magnetopause. The lines along which the position of the propagating shock is tracked in each plane are marked with thick black lines and arrows.

Figure 8 is similar to figure 6 with the horizontal axis extended to include later times. In addition, figure 8 displays the position of the interplanetary shock front close to the magnetopause in the noon-midnight meridian plane (green line) and the ecliptic plane (orange line). While looking at the results in this section, one should keep in mind that the interplanetary magnetic field is mainly in the $y$ direction. Therefore, the draping of the magnetic field lines around the magnetopause occurs in the ecliptic plane ($(xy)$ plane with $z = 0$). The noon-midnight meridian plane ($(xz)$ plane with $y = 0$) can be considered to be perpendicular to the magnetic field.

If we first focus on the orange line in figure 8 we see that, as expected by extrapolating the results from paragraph 3.1.1, the interplanetary shock travels at a reduced speed inside the magnetosheath. However, in the meridian $(xz)$ plane (green line), after a period at reduced velocity (from 216.5 to 226 $\Omega_{ci}^{-1}$), the interplanetary shock accelerates and ends up travelling faster inside the magnetosheath than it does outside.

The result of this asymmetric acceleration/braking on the shape of the interplanetary shock can be apprehended from figure 9, which represents cuts of the current density in the ecliptic plane (left panel) and noon-midnight meridian plane (right panel). Because the part of the interplanetary shock closest to the magnetopause in the $(xy)$ plane is also the one that had the longest time to travel at a decreased speed,

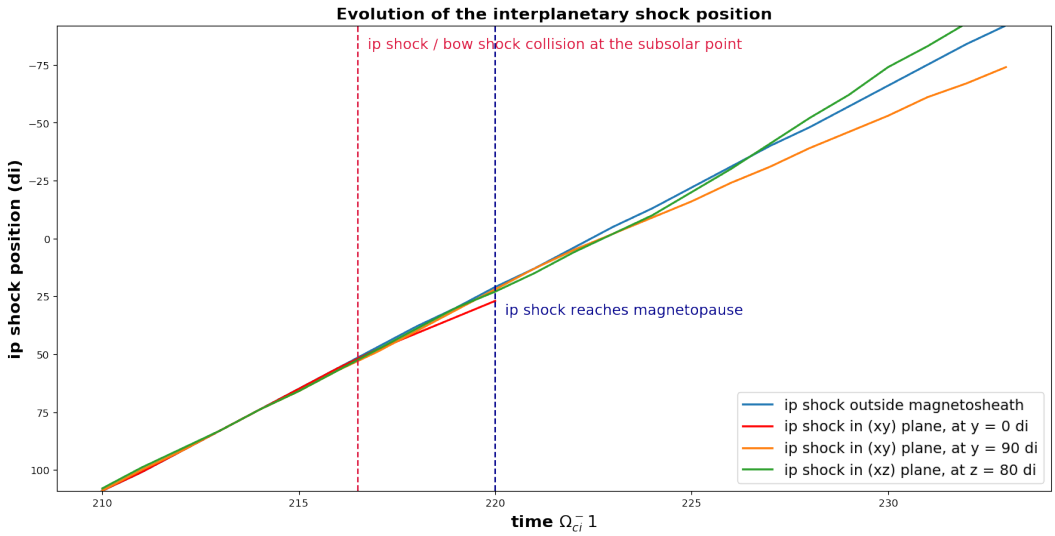


**Figure 8.** Blue line: position of the unperturbed interplanetary shock, as followed outside of the magnetosheath. Red line: position of the interplanetary shock as followed along the Sun-Earth line ($y = z = 0$) until it reaches the magnetopause at $t = 220\ \Omega_{\rm ci}^{-1}$. Green line: position of the interplanetary shock in the noon-midnight meridian plane along the line $y = 0$, $z = 80$. Orange line: position of the interplanetary shock in the equatorial plane along the line $y = 90$, $z = 0$. The two dashed vertical lines indicate the arrival of the interplanetary shock at the nose of the bow shock (red) and, later, at the nose of the magnetosheath (blue)

it lags behind the rest of the interplanetary shock. This leads to a concave shape for the interplanetary shock in the $(xy)$ plane (left panel of figure 9). The opposite is true for the interplanetary shock inside the magnetosheath in the $(xz)$ plane, leading to a roughly convex shape (right panel). We say roughly here because contrarily to the $(xy)$ plane braking, the acceleration in the $(xz)$ plane is efficient only fairly close to the magnetopause rather than across the whole magnetosheath.

We indicated with cyan triangles on figure 9 the locations where we computed $v_s$, the velocity of the interplanetary shock in the GSE frame. To estimate $v_s$, we determine the position of the shock at times 228 to 232 $\Omega_{\rm ci}^{-1}$ and evaluate the slope of the best straight line passing through these points. We then obtain $\tilde{v}_s$, the shock's velocity in the plasma frame, by subtracting from $v_s$ the average plasma bulk velocity in a 5 by 5 $d_i$ cube upstream of the interplanetary shock. These cubes are shown as cyan squares in figure 9.

Koval, Šafránková, Němeček, Samsonov, et al. (2006) have found that, in the observational case they studied, the interplanetary shock's velocity in the bulk plasma frame was constant. This is crucial to their argument that the deceleration of the interplanetary shock is due to the deceleration of the plasma bulk flow. We now examine this proposition in our simulation.

In equations (6) and (7), the subscripts $sw$, $bs$ and $mp$ respectively denote the velocity in the solar wind, in the magnetosheath next to the bow shock, and in the magnetosheath next to the magnetopause. The superscripts $(xy)$ or $(xz)$ reference the plane. The uncertainty for $v_s$ comes from the estimation of the position of the shock, which is limited by the size of the grid cell, of 1 $d_i$. Because we use position estimates spread across 5 $\Omega_{\rm ci}^{-1}$, the error comes down to roughly 1/5 of the nominal Alfvén speed

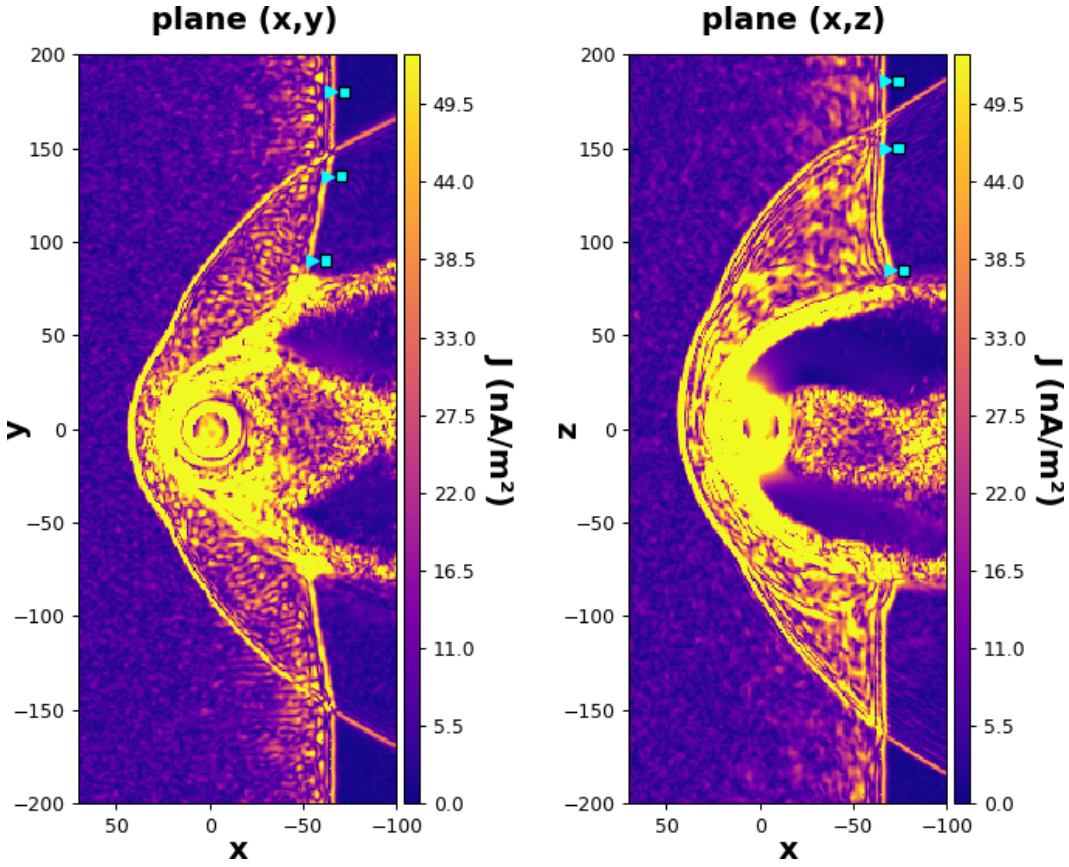


**Figure 9.** Current density during the passage of the shock through the magnetosheath, at time 230 $\Omega_{ci}^{-1}$. Left panel: in the ecliptic plane. Right panel: in the noon-midnight meridian plane. Cyan triangles mark the positions at which the velocity $v_s$ of the shock was measured. Cyan squares upstream of the triangles show areas where the bulk plasma velocity was averaged.

(*i.e.* its value in the solar wind: $v_A \sim 89$ km/s), hence an uncertainty of $\pm 18$ km. The uncertainty for $\tilde{v}_s$ is slightly higher because we take into account the standard variation of the bulk plasma velocity in the 5 by 5 $d_i$ cube used to estimate it.

$$\begin{aligned} v_{s_{sw}}^{(xy)} &= 792 \pm 18 \text{ km/s} & \tilde{v}_{s_{sw}}^{(xy)} &= 387 \pm 21 \text{ km/s} \\ v_{s_{bs}}^{(xy)} &= 660 \pm 18 \text{ km/s} & \tilde{v}_{s_{bs}}^{(xy)} &= 361 \pm 24 \text{ km/s} \\ v_{s_{mp}}^{(xy)} &= 645 \pm 18 \text{ km/s} & \tilde{v}_{s_{mp}}^{(xy)} &= 387 \pm 28 \text{ km/s} \end{aligned} \tag{6}$$

$$\begin{aligned} v_{s_{sw}}^{(xz)} &= 782 \pm 18 \text{ km/s} & \tilde{v}_{s_{sw}}^{(xz)} &= 379 \pm 22 \text{ km/s} \\ v_{s_{bs}}^{(xz)} &= 760 \pm 18 \text{ km/s} & \tilde{v}_{s_{bs}}^{(xz)} &= 424 \pm 23 \text{ km/s} \\ v_{s_{mp}}^{(xz)} &= 911 \pm 18 \text{ km/s} & \tilde{v}_{s_{mp}}^{(xz)} &= 422 \pm 37 \text{ km/s} \end{aligned} \tag{7}$$

The estimates of $v_s$ (left column) clearly show the acceleration/braking on the interplanetary shock in the $(xz)/(xy)$ plane ($v_{s_{mp}}^{(xz)}$ is markedly larger than $v_{s_{mp}}^{(xy)}$). Furthermore, the estimates of $\tilde{v}_s$ (right column) align with Koval, Šafránková, Němeček, Samsonov, et al. (2006)'s observation that the shock speed in the plasma frame does not significantly vary when the shock penetrates the magnetosheath.

### 3.2 Turning into a quasi-parallel propagating shock

Figure 10 represents the magnetic field lines (white arrows) superimposed on the magnetic field amplitude in the ecliptic plane. The draping of the magnetic field lines around the magnetopause leads to a significant $x$ component of the magnetic field in the $(xy)$ plane. Therefore, when the interplanetary shock travels through the magnetosheath, while it is quasi-perpendicular in most places, it is quasi-parallel in the $(xy)$ plane close to the magnetopause. For example, in the magnetosheath close to the magnetopause in the ecliptic plane, we measured that the angle between the normal of the shock with the upstream magnetic field was $\theta_{Bn} \sim 31°$, even though $\theta_{Bn} \sim 85°$ in the solar wind. We do not expect the same effect in the $(xz)$ plane because the magnetic field lines slip along the obstacle and there is no draping.

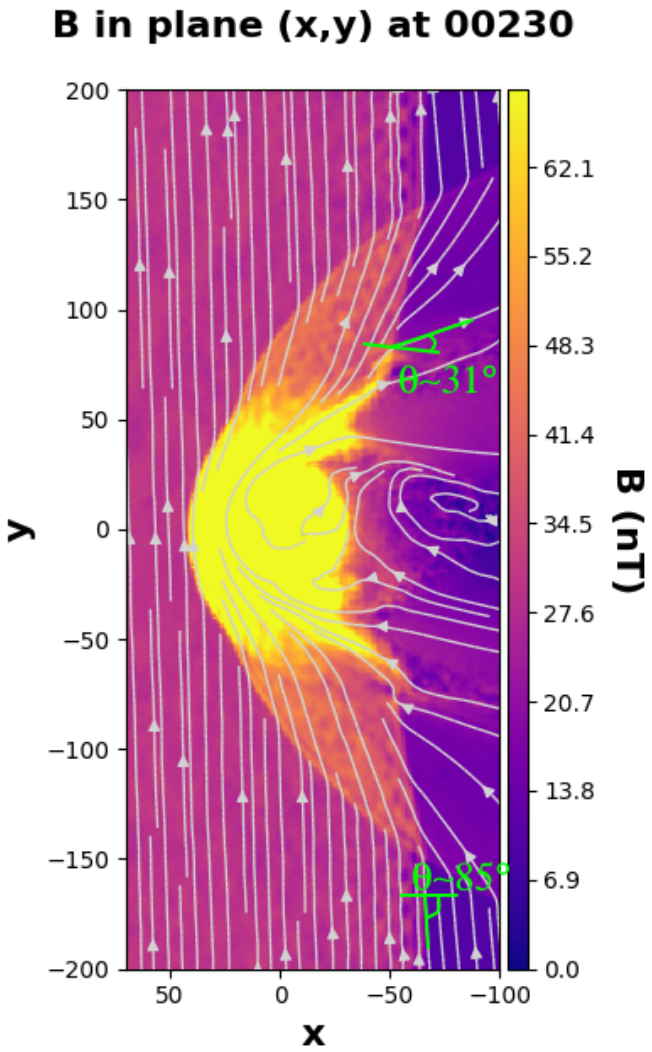


**Figure 10.** Colors: Magnetic field amplitude. White lines: magnetic field lines. The figure is made at time 230 $\Omega_{ci}^{-1}$ in the ecliptic plane. In green, at two different locations, we show the shock's normal and the direction of the magnetic field lines. The angle between these two lines is marked.

## 4 Discussion

In section 3.1, we described how some parts of the interplanetary shock could be accelerated as it travels through the magnetosheath. This seems to go against previous studies on the subject (*e.g.* Villante et al. (2004); Koval et al. (2005); Koval, Šafránková, Němeček, Samsonov, et al. (2006); Samsonov et al. (2006)) which concluded that interplanetary shocks would decelerate in the magnetosheath. Yet, we can logically infer the acceleration of the interplanetary shock from a passing conclusion from Koval, Šafránková, Němeček, Samsonov, et al. (2006). Indeed, the authors observed in a case study that the interplanetary shock's velocity was constant in the plasma frame. If we acknowledge the fact that the plasma bulk flow can accelerate in some places of the magnetosheath (*e.g.* Chen et al. (1993); Lavraud et al. (2007, 2013)), then it follows that it should be possible for the interplanetary shock to be accelerated in the magnetosheath.

In section 3.1.2, we have shown that Koval, Šafránková, Němeček, Samsonov, et al. (2006)'s observation of the conservation of the interplanetary shock's velocity in the plasma frame was indeed valid wherever we tested it in our simulation. A toy model can help us see why. Using the first Rankine Hugoniot equation, we can define the velocity of the shock as $v_s = \frac{n_u v_u - n_d v_d}{n_u - n_d}$, where $n_u$ and $v_u$ represent the plasma density and bulk velocity upstream of the travelling shock, and $n_d$ and $v_d$ the same quantities downstream of the travelling shock.

$$\tilde{v}_s = \frac{n_u v_u - n_d v_d}{n_u - n_d} - v_u = \frac{n_d \times (v_u - v_d)}{n_u - n_d} \tag{8}$$

Let us assume that both $v_u$ and $v_d$ change by a quantity $\Delta v$, which could be the case, for example, when the interplanetary shock penetrates inside the magnetosheath; then we see immediately that $\tilde{v}_s$ is not modified.

Since our simulation indeed reproduces the acceleration of the bulk plasma on the flanks of the magnetopause in the plane orthogonal to the interplanetary magnetic field, this allowed us not only to observe that the interplanetary shock was accelerated but also to understand why. From this same toy model it is easy to see why the acceleration/deceleration of the plasma itself might lead to an acceleration/deceleration of the shock travelling in it. Let us assume that the plasma in the magnetopause is changed on both sides of the travelling shock by the same quantity $\Delta v$. We can then write the new shock velocity $v_s'$ as:

$$v_s' = \frac{n_u(v_u + \Delta v) - n_d(v_d + \Delta v)}{n_u - n_d} = v_s + \Delta v \tag{9}$$

The sign of $\Delta v$ controls the acceleration/braking of the interplanetary shock: a slow plasma bulk flow in the plane of the interplanetary magnetic field leads to a deceleration of the interplanetary shock in the magnetosheath; a fast plasma bulk flow in the plane orthogonal to the interplanetary magnetic field leads to an acceleration of the interplanetary shock in the magnetosheath.

This explanation may help us understand why there is such a large difference between the conclusions of (Villante et al., 2004)'s and (Koval, Šafránková, Němeček, & Přech, 2006). (Villante et al., 2004) used the satellite Wind to detect the interplanetary shocks. Then the authors inferred the time at which the shocks would reach the bow shock and compare this time with the time of ground measurements of associated disturbances. This silently implies that the speed of the interplanetary shock through the magnetosheath being inferred is the speed of the interplanetary shock through the nose of the magnetosheath; where the bulk plasma flow is by and large the slowest. The average shock speed in (Villante et al., 2004) was around 350 km/s. Assuming that the solar wind itself has a speed of around 300 km/s and that the bulk plasma in the nose of the magnetosheath would have an average velocity of 50 km/s, our toy

model would predict that the shock would propagate at a constant speed of 50 km/s in the plasma frame, *i.e.* a speed of 100 km/s in the magnetosheath, versus 350 km/s in the solar wind. This would be understood as: in the magnetosheath, the shock travels at $100/350 \sim 0.29$ times its velocity in the solar wind, which was the authors conclusion. Now, if we look at figure 1 of (Koval, Šafránková, Němeček, & Přech, 2006), we see that the observations concern a shock propagating through the flank of the magnetosheath, where the bulk plasma flows much faster. Using figure 2 of (Koval, Šafránková, Němeček, & Přech, 2006), we can estimate that the shock speed in the solar wind was 440 km/s, and that – relative to the plasma frame – it was 80 km/s. Inside of the magnetosheath, we can see that the bulk plasma flows at 300 km/s. Inside of the magnetosheath, the shock would therefore travel (using our toy model) at a speed of 380 km/s. This would be understood as: in the magnetosheath, the shock travels at $380/440 \sim 0.86$ times its velocity in the solar wind.

We can draw two conclusions from this: the first is that we should forego of the idea that an interplanetary shock – which has a single well defined velocity in the solar wind – also has a single well defined velocity in the magnetosheath. The absolute velocity of the interplanetary shock highly depends on the velocity of the bulk plasma, which in turns highly depends on where in the magnetosheath we are looking. The second conclusion is that thinking about the change of speed of the interplanetary shock in terms of a multiplication by a certain factor can be quite misleading. Perhaps we should rather think in terms of subtraction (*i.e.* the shock slowed down by x km/s), or simply in terms of locally defined Mach numbers (*i.e.* $(v_{shock} - v_{plasma})$ divided by a characteristic speed).

One last remark on figure 8: in the meridian plane ($xz$), the shock was actually slowed down at first when entering the magnetosheath and started to accelerate only when it reaches the flanks of the magnetosheath. As shown by (Chen et al., 1993; Lavraud et al., 2007, 2013), the plasma bulk flow is faster in the magnetosheath than it is in the solar wind on the flanks; but still slower just behind the bow shock. Hence, it natural (according to our toy model) that the interplanetary shock would first slow down, then accelerate.

In the previous discussion, all of our arguments drew on magnetohydrodynamics concepts. We are therefore drawn to the same conclusion as (Koval, Šafránková, Němeček, Samsonov, et al., 2006): kinetic effects seem to play at most a minor role in the particular question of deceleration/acceleration of interplanetary shocks through the magnetosheath.

However, this should not lead us to rule out kinetic effects from the larger question of the interaction between interplanetary shocks and the geomagnetic environment. In fact, we have seen in section 3.2 that a quasi-perpendicular shock in the solar wind could turn into a quasi-parallel shock inside of the magnetosheath. Collisionless quasi-parallel shocks can only be rigorously simulated by including kinetic physics. While we cannot point yet to any clear consequence this might have, we believe that it is worth noting. Indeed, we can understand from figure 10 that any interplanetary shock travelling through the magnetosheath is likely to have parts of it in a quasi-parallel shock scenario.

We believe that this quasi-parallel situation is at the origin of two current structures visible on the left panel of figure 9 at the places where the interplanetary shock intersects the magnetopause. Macro-particles accelerated at the interplanetary shock close to magnetopause can travel along the magnetic field lines since they are almost parallel to the shock's normal. In our simulation, some of these particles actually cross the magnetopause. The density being fairly low there, the electric field is probably over-estimated by our hybrid scheme, which may lead these particles to be accelerated to velocities larger than they would in reality, which in turn leads to strong currents

that may not be realistic. Moreover, by reducing the size of the geomagnetic environment while keeping the solar wind scales the same as in reality, our code is bound to overestimate kinetic effects. However, while we cannot yet conclude on the amplitude of these effects in observations, we argue that a magnetohydrodynamic approach will inevitably miss them entirely.

## 5 Conclusion

In our Hybrid PIC simulations of the self-consistent interaction between an interplanetary shock and the geomagnetic environment, we found that asymmetry of the plasma velocity in the magnetosheath could modify the curvature of the interplanetary shock in a non-trivial way: accordingly to previous studies (*e.g.* Koval et al. (2005); Koval, Šafránková, Němeček, Samsonov, et al. (2006); Koval, Šafránková, Němeček, and Přech (2006); Samsonov et al. (2006); Šafránková et al. (2007); Pallocchia et al. (2010)) we found that parts of the shock are slowed down during their propagation through the magnetosheath; however, our simulation show that others are accelerated. The acceleration occurs in the flanks of the magnetosheath in the plane perpendicular to the interplanetary magnetic field. We argued that the shock is accelerated there because it "rides on" a faster bulk plasma, itself in the right conditions to be accelerated by the Lorentz force (Chen et al., 1993; Lavraud et al., 2007, 2013).

The peculiar shape of the interplanetary shock (from convex in the $(xy)$ plane to concave in the $(xz)$ plane), as well as the possibility to accelerate particles close to the magnetopause, might significantly affect the solar wind/magnetosphere coupling processes on the flanks of the magnetosheath, and possibly further along the magnetotail. The question of the geoeffectiveness of shocks is not completely closed.

In the near future, an observational study of the type made by Koval et al. (2005) and Koval, Šafránková, Němeček, and Přech (2006) could potentially look for interplanetary shocks encounters in the magnetosheath which, rather than arriving with a delay compared to a constant speed in the solar wind, could arrive with an advance. We predict that this is more likely to be observed during an interval of solar wind with low $\beta$ carrying an interplanetary magnetic field with relatively constant direction and in the plane orthogonal to the latter (Lavraud et al., 2007). These relatively restrictive conditions explain why Koval et al. (2005) and Koval, Šafránková, Němeček, and Přech (2006) only found a small number of shocks that seemed to travel faster in the magnetosheath than in the solar wind, which they discarded from their analysis because of lack of measurement precision.

Using figure 8, we can make a rough estimate of the expected delay/advance of the detection of the interplanetary shock by a satellite that would be placed at $17R_E$ downstream of Earth (corresponding to $-75$ $d_i$ in our simulation), near the magnetopause in the magnetosheath:

- If the satellite is in the same plane as the interplanetary magnetic field (ecliptic plane (xy) in our simulation), we would expect the interplanetary shock to be decelerated, resulting in a delay of 32 seconds (the simulated delay is 2 $\Omega_{\mathrm{ci}}^{-1}$, times the scaling factor 16) compared to a constant-velocity interplanetary shock.
- If the satellite is in the plane perpendicular to the interplanetary magnetic field (noon-midnight meridian plane (xz) in our simulation), we would expect the interplanetary shock to be accelerated, resulting in an advance of 16 seconds (the simulated advance is 1 $\Omega_{\mathrm{ci}}^{-1}$, times the scaling factor 16) compared to a constant-velocity interplanetary shock.

We have also suggested the possibility of seeing accelerated particles at the intersection of the magnetopause and the interplanetary shock in the plane of the interplanetary

magnetic field. However, we do not know how large this effect might be in reality, as our simulation lacks the phase space resolution to describe it properly. It may be worth using satellite data to look for accelerated particles in the plane of the interplanetary magnetic field, next to the magnetopause, upstream of an interplanetary shock travelling through the magnetosheath.

**Acknowledgments**
This work received financial support from the "Investissements d'avenir" program under the reference ANR-11-IDEX-0004-02 (Plas@Par). We are indebted to the ANR for the project TEMPETE (ANR-17-CE31-0016). We were granted access to the HPC resources of IDRIS under the allocation 2021-A0090410276 made by GENCI.

## References

Burlaga, L. F. (1988). Magnetic clouds and force-free fields with constant alpha. *Journal of Geophysical Research*, *93*(A7), 7217. doi: 10.1029/JA093iA07p07217

Chen, S.-H., Kivelson, M. G., Gosling, J. T., Walker, R. J., & Lazarus, A. J. (1993). Anomalous aspects of magnetosheath flow and of the shape and oscillations of the magnetopause during an interval of strongly northward interplanetary magnetic field. *Journal of Geophysical Research: Space Physics*, *98*(A4), 5727–5742. doi: 10.1029/92JA02263

Dungey, J. W. (1961, January). Interplanetary Magnetic Field and the Auroral Zones. *Physical Review Letters*, *6*(2), 47–48. doi: 10.1103/PhysRevLett.6.47

Fairfield, D. H., & Cahill, L. J. (1966). Transition region magnetic field and polar magnetic disturbances. *Journal of Geophysical Research (1896-1977)*, *71*(1), 155–169. doi: 10.1029/JZ071i001p00155

Kilpua, E. K. J., Koskinen, H. E. J., & Pulkkinen, T. I. (2017, December). Coronal mass ejections and their sheath regions in interplanetary space. *Living Reviews in Solar Physics*, *14*(1). doi: 10.1007/s41116-017-0009-6

Koval, A., Šafránková, J., Němeček, Z., & Přech, L. (2006, January). Propagation of interplanetary shocks through the solar wind and magnetosheath. *Advances in Space Research*, *38*(3), 552–558. doi: 10.1016/j.asr.2006.05.023

Koval, A., Šafránková, J., Němeček, Z., Přech, L., Samsonov, A. A., & Richardson, J. D. (2005). Deformation of interplanetary shock fronts in the magnetosheath. *Geophysical Research Letters*, *32*(15). doi: 10.1029/2005GL023009

Koval, A., Šafránková, J., Němeček, Z., Samsonov, A. A., Přech, L., Richardson, J. D., & Hayosh, M. (2006, June). Interplanetary shock in the magnetosheath: Comparison of experimental data with MHD modeling. *Geophysical Research Letters*, *33*, L11102. doi: 10.1029/2006GL025707

Lavraud, B., Borovsky, J. E., Ridley, A. J., Pogue, E. W., Thomsen, M. F., Rème, H., ... Lucek, E. A. (2007, July). Strong bulk plasma acceleration in Earth's magnetosheath: A magnetic slingshot effect? *Geophysical Research Letters*, *34*(14), L14102. doi: 10.1029/2007GL030024

Lavraud, B., Larroque, E., Budnik, E., Génot, V., Borovsky, J. E., Dunlop, M. W., ... Rème, H. (2013). Asymmetry of magnetosheath flows and magnetopause shape during low Alfvén Mach number solar wind. *Journal of Geophysical Research: Space Physics*, *118*(3), 1089–1100. doi: 10.1002/jgra.50145

Lepping, R. P., Berdichevsky, D. B., Wu, C.-C., Szabo, A., Narock, T., Mariani, F., ... Quivers, A. J. (2006, March). A summary of WIND magnetic clouds for years 1995-2003: Model-fitted parameters, associated errors and classifications. *Annales Geophysicae*, *24*(1), 215–245. doi: 10.5194/angeo-24-215-2006

Lin, N., Engebretson, M. J., McPherron, R. L., Kivelson, M. G., Baumjohann, W., Luehr, H., ... Zanetti, L. J. (1991). A comparison of ULF fluctuations in the

solar wind, magnetosheath, and dayside magnetosphere: 2. Field and plasma conditions in the magnetosheath. *Journal of Geophysical Research: Space Physics*, *96*(A3), 3455–3464. doi: 10.1029/90JA02098

Lucek, E. A., Constantinescu, D., Goldstein, M. L., Pickett, J., Pinçon, J. L., Sahraoui, F., ... Walker, S. N. (2005, June). The Magnetosheath. *Space Science Reviews*, *118*(1-4), 95–152. doi: 10.1007/s11214-005-3825-2

Modolo, R. (2004). *Modélisation de l'interaction du vent solaire, ou du plasma Kronien, avec les environnements neutres de Mars et de Titan* (These de Doctorat). Versailles-St Quentin en Yvelines.

Moissard, C., Fontaine, D., & Savoini, P. (2019). A Study of Fluctuations in Magnetic Cloud-Driven Sheaths. *Journal of Geophysical Research: Space Physics*, *124*(11), 8208–8226. doi: 10.1029/2019JA026952

Omidi, N., Blanco-Cano, X., Russell, C., & Karimabadi, H. (2004, January). Dipolar magnetospheres and their characterization as a function of magnetic moment. *Advances in Space Research*, *33*(11), 1996–2003. doi: 10.1016/j.asr.2003.08.041

Pallocchia, G., Samsonov, A. A., Bavassano Cattaneo, M. B., Marcucci, M. F., Rème, H., Carr, C. M., & Cao, J. B. (2010, May). Interplanetary shock transmitted into the Earth's magnetosheath: Cluster and Double Star observations. *Annales Geophysicae*, *28*(5), 1141–1156. doi: 10.5194/angeo-28-1141-2010

Regnault, F., Janvier, M., Dèmoulin, P., Auchére, F., Strugarek, A., Dasso, S., & Noûs, C. (2020). 20 Years of ACE Data: How Superposed Epoch Analyses Reveal Generic Features in Interplanetary CME Profiles. *Journal of Geophysical Research: Space Physics*, *n/a*(n/a), e2020JA028150. doi: 10.1029/2020JA028150

Šafránková, J., Němeček, Z., Přech, L., Samsonov, A. A., Koval, A., & Andréeová, K. (2007, August). Modification of interplanetary shocks near the bow shock and through the magnetosheath: INTERPLANETARY SHOCKS NEAR THE BOW SHOCK. *Journal of Geophysical Research: Space Physics*, *112*(A8), n/a-n/a. doi: 10.1029/2007JA012503

Samsonov, A. A., Němeček, Z., & Šafránková, J. (2006). Numerical MHD modeling of propagation of interplanetary shock through the magnetosheath. *Journal of Geophysical Research*, *111*(A8). doi: 10.1029/2005JA011537

Samsonov, A. A., Sibeck, D. G., & Imber, J. (2007, December). MHD simulation for the interaction of an interplanetary shock with the Earth's magnetosphere: INTERPLANETARY SHOCK. *Journal of Geophysical Research: Space Physics*, *112*(A12), n/a-n/a. doi: 10.1029/2007JA012627

Schield, M. A. (1969). Pressure balance between solar wind and magnetosphere. *Journal of Geophysical Research (1896-1977)*, *74*(5), 1275–1286. doi: 10.1029/JA074i005p01275

Spreiter, J. R., & Stahara, S. S. (1992). Computer Modeling of Solar Wind Interaction With Venus and Mars. In *Venus and Mars: Atmospheres, Ionospheres, and Solar Wind Interactions* (pp. 345–383). American Geophysical Union (AGU). doi: 10.1029/GM066p0345

Spreiter, J. R., & Stahara, S. S. (1994, July). Gasdynamic and magnetohydrodynamic modeling of the magnetosheath: A tutorial. *Advances in Space Research*, *14*(7), 5–19. doi: 10.1016/0273-1177(94)90042-6

Tsurutani, B. T., Lakhina, G. S., & Hajra, R. (2020, February). The physics of space weather/solar-terrestrial physics (STP): What we know now and what the current and future challenges are. *Nonlinear Processes in Geophysics*, *27*(1), 75–119. doi: 10.5194/npg-27-75-2020

Turc, L., Fontaine, D., Savoini, P., & Modolo, R. (2015, August). 3D hybrid simulations of the interaction of a magnetic cloud with a bow shock: SIMULATIONS OF MC/BOW SHOCK INTERACTION. *Journal of Geophysical Research: Space Physics*, *120*(8), 6133–6151. doi: 10.1002/2015JA021318

Venzmer, M. S., & Bothmer, V. (2018, March). Solar-wind predictions for the Parker Solar Probe orbit - Near-Sun extrapolations derived from an empirical solar-wind model based on Helios and OMNI observations. *Astronomy & Astrophysics*, *611*, A36. doi: 10.1051/0004-6361/201731831

Villante, U., Lepidi, S., Francia, P., & Bruno, T. (2004, March). Some aspects of the interaction of interplanetary shocks with the Earth's magnetosphere: An estimate of the propagation time through the magnetosheath. *Journal of Atmospheric and Solar-Terrestrial Physics*, *66*(5), 337–341. doi: 10.1016/j.jastp.2004.01.003